

Decoding millimetre-wave spectra of 2-iminopropanenitrile, a candidate for astronomical observations

K. Luková, L. Kolesnikova, J. Koucký, K. Vávra, P. Kania, Jean-Claude Guillemin, S Urban

▶ **To cite this version:**

K. Luková, L. Kolesnikova, J. Koucký, K. Vávra, P. Kania, et al.. Decoding millimetre-wave spectra of 2-iminopropanenitrile, a candidate for astronomical observations. Astronomy and Astrophysics - A&A, 2022, 665, pp.A9. 10.1051/0004-6361/202243696 . hal-03797289

HAL Id: hal-03797289
https://hal.science/hal-03797289

Submitted on 4 Oct 2022

HAL is a multi-disciplinary open access archive for the deposit and dissemination of scientific research documents, whether they are published or not. The documents may come from teaching and research institutions in France or abroad, or from public or private research centers.

L'archive ouverte pluridisciplinaire **HAL**, est destinée au dépôt et à la diffusion de documents scientifiques de niveau recherche, publiés ou non, émanant des établissements d'enseignement et de recherche français ou étrangers, des laboratoires publics ou privés.



Distributed under a Creative Commons Attribution 4.0 International License

A&A 665, A9 (2022)
https://doi.org/10.1051/0004-6361/202243696
© K. Luková et al. 2022

Astronomy & Astrophysics

Decoding millimetre-wave spectra of 2-iminopropanenitrile, a candidate for astronomical observations*

K. Luková[1], L. Kolesniková[1], J. Koucký[1], K. Vávra[1], P. Kania[1], J.-C. Guillemin[2], and Š. Urban[1]

[1] Department of Analytical Chemistry, University of Chemistry and Technology, Technická 5, 166 28 Prague 6, Czech Republic
e-mail: Katerina.Lukova@vscht.cz, Lucie.Kolesnikova@vscht.cz
[2] Univ Rennes, Ecole Nationale Supérieure de Chimie de Rennes, CNRS, ISCR – UMR 6226, 35000 Rennes, France

Received 1 April 2022 / Accepted 1 June 2022

ABSTRACT

Aims. The recent detection of cyanomethanimine in the interstellar medium makes its methyl derivative, 2-iminopropanenitrile ($CH_3C(CN)NH$), a promising candidate for an interstellar detection. The aim of this work is to extend the current knowledge of the laboratory rotational spectrum to higher frequencies, which is an essential prerequisite for an identification of the molecular species in the interstellar medium by millimetre-wave astronomy.

Methods. The room-temperature rotational spectrum of 2-iminopropanenitrile has been measured in several frequency regions between 128 and 329 GHz. The *A*–*E* splittings of the rotational transitions arising from the methyl top internal rotation were analysed employing the ERHAM and XIAM programs.

Results. A dataset of approximately 900 newly assigned rotational transitions in the ground state of the *Z* isomer and a set of refined molecular constants, including the internal rotation parameters, are reported. Moreover, this work provides the first spectral characterisation of the less stable *E* isomer ground state, as well as the three lowest-lying vibrationally excited states of the *Z* isomer, $v_{21} = 1$, $v_{14} = 1$, and $v_{20} = 1$. This comprehensive spectroscopic study will allow a search for 2-iminopropanenitrile in the millimetre-wave surveys of interstellar sources, such as those recorded by the Atacama Large Millimeter/submillimeter Array.

Key words. astrochemistry – molecular data – methods: laboratory: molecular – techniques: spectroscopic – ISM: molecules

1. Introduction

One of the most attractive targets of current astrochemistry are complex organic molecules, astrophysically relevant organic compounds that contain at least six atoms (Herbst & van Dishoeck 2009), as they are considered to be precursors of important prebiotic species. Therefore, the identification of their spectral transitions in the interstellar medium (ISM) provides valuable insight not only into chemical and physical conditions of the environments, where they reside, but also into the chemical evolution and formation of stars and new planetary systems (e.g. Herbst & van Dishoeck 2009; Garrod et al. 2008).

To date, about 90 complex organic molecules have been detected in the ISM, and the vast majority of them have been detected thanks to a synergistic relationship between radio-astronomical techniques and rotational spectroscopy, which provides accurate laboratory reference spectra of candidate molecules that serve as a guidance tool. N-bearing molecules are particularly widely distributed in miscellaneous types of the ISM. Among them, nitriles – plausible key players in the formation of amino acids, peptides, and nucleic acids (see e.g. Balucani 2009; Bernstein et al. 2002; Powner et al. 2010 and references therein) – constitute a significant fraction of more than 25%. In addition, a large dipole moment of nitriles results in strong rotational spectra and facilitates their interstellar observations (McGuire 2022).

The most recent detections from the CN-bearing family include molecular species such as propargylcyanide (McGuire et al. 2020), cyanopentaacetylene (Loomis et al. 2021), cyanovinylacetylene, vinylcyanoacetylene (Lee et al. 2021b), *n*-propyl cyanide (Garrod et al. 2009), and the first detected branched molecule, iso-propyl cyanide (Belloche et al. 2014). An eminent success was the detections of aromatic nitriles: benzonitrile (McGuire et al. 2018) and the very recent observations of the isomeric pairs 1-cyano-1,3-cyclopentadiene (McCarthy et al. 2021) and 2-cyano-1,3-cyclopentadiene (Lee et al. 2021a) and the polycyclic aromatic hydrocarbons 1-cyanonaphtalene and 2-cyanonaphtalene (McGuire et al. 2021). Dinitriles have also gained the attention of spectroscopists in the context of radio-astronomical observations (see e.g. Motiyenko et al. 2019; Cabezas et al. 2020). The great diversity across the interstellar nitriles can also be demonstrated on molecules that bear two different functional groups, such as aminoacetonitrile (Belloche et al. 2008), cyanomethanimine (Zaleski et al. 2013; Melosso et al. 2018), and glycolonitrile (Zeng et al. 2019). Consequently, nitriles are nowadays of great astrophysical significance, and many more CN-functionalised species are yet to be searched for, as their laboratory spectroscopic characterisations have already been carried out, for example cyanoacetamide (Sanz-Novo et al. 2020), cyanoacetic acid (Sanz-Novo et al. 2021), aminocyanoacetylene (Kolesniková et al. 2021), phenylpropiolonitrile (Buchanan et al. 2021), 9-cyanoanthracene and 9-cyanophenanthrene (McNaughton et al. 2018), 1-cyano-1,3-butadiene, and 4-cyano-1,2-butadiene (Zdanovskaia et al. 2021).

Here we present a comprehensive rotational study of a potential candidate for astronomical search, 2-iminopropanenitrile

* Full Tables A.3 and A.4 are only available at the CDS via anonymous ftp to cdsarc.u-strasbg.fr (130.79.128.5) or via http://cdsarc.u-strasbg.fr/viz-bin/cat/J/A+A/665/A9

Open Access article, published by EDP Sciences, under the terms of the Creative Commons Attribution License (https://creativecommons.org/licenses/by/4.0), which permits unrestricted use, distribution, and reproduction in any medium, provided the original work is properly cited.
This article is published in open access under the Subscribe-to-Open model. Subscribe to A&A to support open access publication.

(hereafter IPN), a nine-atom molecule featuring a large amplitude motion linked to a hindered internal rotation of a methyl group. Our investigation was motivated by the recent detection of cyanomethanimine (HNCHCN), a methyl-shortened structural analogue of IPN. In total, eight rotational transitions of the less stable *E* form of HNCHCN were detected in the frequency range 9–50 GHz towards the star-forming region Sagittarius B2(N) by Zaleski et al. (2013). In 2018, aided by laboratory spectroscopic studies by Takano et al. (1990), Zaleski et al. (2013), and Melosso et al. (2018), the rotational transitions of both the *E* and *Z* form were detected at higher frequencies of 84–110 GHz towards the Galactic Centre quiescent molecular cloud G+0.693 (Rivilla et al. 2019).

In this work, we follow up on the previous study of Groner et al. (1987), in which two possible stable isomers, *Z* and *E* (see Fig. 1), were proposed for IPN on the basis of ab initio calculations. However, only the rotational spectrum of the more stable *Z* isomer in its ground vibrational state was recorded in the frequency region 19–51 GHz. Nevertheless, extrapolating from the microwave spectral window often results in inaccurate predictions at higher frequencies. Hence, laboratory data from these high frequency regions are necessary for an effective guiding of interstellar searches for IPN by millimetre-wave astronomy. In this context, we measured its rotational spectrum in several frequency regions from 128 to 329 GHz, which was followed by a thorough analysis of the *A*–*E* splittings of the rotational transitions due to the presence of a methyl internal top in the molecule. In addition to the *Z*-form ground vibrational state, its three lowest-lying vibrationally excited states, $v_{21} = 1$, $v_{14} = 1$, and $v_{20} = 1$, were identified. Furthermore, the rotational spectrum of the less stable *E* isomer in its ground vibrational state is reported for the first time. The spectral analysis presented here allows the strongest observed lines in the millimetre-wave spectrum of IPN to be reproduced close to the experimental uncertainty and might enable future astronomical observations of this species in the ISM.

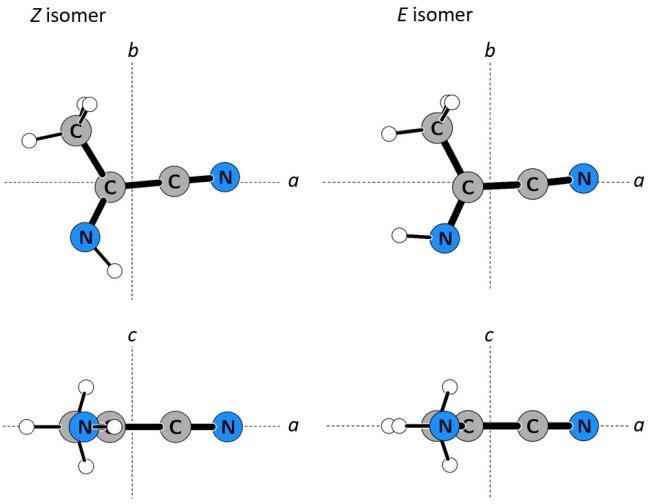


Fig. 1. Molecular structures of the *Z* and *E* isomer of IPN calculated at the DFT/B3LYP/6-311++G(2d,3p) level of theory displayed in the *ab* and *ac* inertial planes.

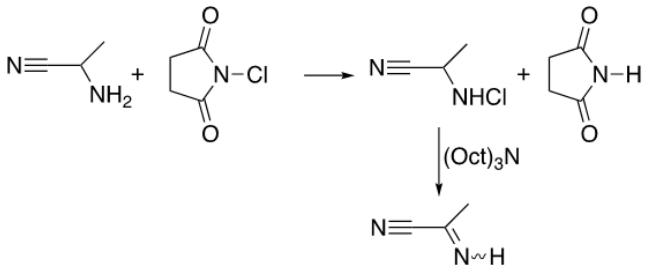


Fig. 2. Synthesis of IPN.

2. Experimental details

2.1. Synthesis

N-chlorosuccinimide (2.7 g, 20 mmol) and bis(2-butoxyethyl) ether (40 ml) were introduced into a three-necked flask equipped with a stirring bar. The flask was connected to a vacuum line and evacuated (0.1 mbar), and then immersed in a bath cooled to −40 °C. 2-Aminopropanenitrile (1.4 g, 20 mmol) was added through a septum. The mixture was stirred at room temperature for 15 min, the flask was then cooled again to −40 °C, and trioctylamine in excess (5 mL, 11.4 mmol) was added (Fig. 2). The mixture was stirred at room temperature for 30 min while the imine was distilled under vacuum and trapped in a U-tube immersed in a bath cooled to −70 °C. IPN was kept cooled in a liquid nitrogen bath to prevent polymerisation. The sample was used without further purification. The yield was 43%.

2.2. Measurement of spectra

The room-temperature rotational spectra were measured in the frequency regions 128–144, 180–218, and 282–329 GHz, using the upgraded Prague semiconductor millimetre-wave spectrometer (Kania et al. 2006). The required frequencies were achieved by multiplying the fundamental frequency (<50 GHz) produced by the Agilent E8257D synthesiser using different amplifier-multiplier chains with multiplication factors of 4, 8, and 12. The fundamental frequency was modulated at a frequency of 28 kHz and a depth of between 40 and 60 kHz. The double-pass configuration was implemented to increase the optical path length to 4.6 m via a rooftop mirror. The signal was then detected by a zero-bias detector and demodulated by a lock-in amplifier tuned to twice the modulation frequency. Further details about the spectrometer have been given elsewhere (Kania et al. 2006). The evacuated absorption cell was filled with the sample to the absolute pressure of 15–30 μbar. When the intensity of a selected line decreased by approximately 50%, the cell was evacuated and then filled with the sample again. Attempts to establish a slow flow through the cell were unfruitful due to the very low vapour pressure of the sample. The measured frequencies were averaged from scans measured in the direction of increasing and decreasing frequency, respectively. The experimental uncertainty of the isolated symmetrical well-developed line was estimated to be 30 kHz, and uncertainties of 50 kHz were given to broader and blended lines or in the case of a poor signal-to-noise ratio.

3. Computational details

Although some structural molecular parameters of both *Z*-IPN and *E*-IPN were calculated and reported in previous studies by Groner et al. (1987) and more recently by Durig et al. (2010), we undertook our own quantum-chemical calculations of the spectroscopic parameters relevant to this work. Hence, we performed geometry optimisations of both isomers followed by the calculations of second analytical derivatives as well as finite differences to compute a cubic force field. The harmonic and anharmonic

Table 1. Predicted and experimentally determined spectroscopic parameters of the *Z* and *E* isomer in the ground state (*A* reduction, I^r representation).

	Z isomer			*E* isomer	
Parameters	Calculated [a]	Groner et al. (1987)	This work	Calculated [a]	This work
A/MHz	9774.223	9812.1614(54)	9812.1796(15) [b]	9741.906	9781.9611(59)
B/MHz	4176.409	4168.2347(29)	4168.22656(17)	4196.015	4189.31394(48)
C/MHz	2975.830	2975.1826(29)	2975.16898(21)	2982.875	2983.20974(68)
Δ_J/kHz	0.751	0.859(32)	0.77395(15)	0.743	0.765934(93)
Δ_{JK}/kHz	14.628	15.75(12)	15.66422(61)	14.012	15.0050(19)
Δ_K/kHz	–4.952	–7.00(52)	–5.837(12)	–4.767	–5.675(22)
δ_J/kHz	0.249	0.2687(39)	0.258324(29)	0.244	0.253809(61)
δ_K/kHz	8.799	9.028(72)	9.4666(15)	8.348	8.9534(44)
Φ_J/mHz	0.356	–	0.526(40)	0.324	[0.324] [c]
Φ_{JK}/Hz	0.131	–	0.1491(14)	0.114	0.12429(63)
Φ_{KJ}/Hz	–0.278	–	–0.3298(49)	–0.222	–0.2517(26)
Φ_K/Hz	0.191	–	[0.191] [c]	0.132	[0.132] [c]
ϕ_J/mHz	0.180	–	[0.180] [c]	0.158	[0.158] [c]
ϕ_{JK}/Hz	0.067	–	0.07646(65)	0.059	0.0638(11)
ϕ_K/Hz	0.296	–	0.361(10)	0.269	[0.269] [c]
ϵ_{10}/MHz	–	–	–17.416(31)	–	–35.698(63)
$[(B-C)/4]_{10}$/kHz	–	–	–	–	0.223(35)
$[(B+C)/2]_{10}$/kHz	–	–	–	–	0.810(59)
ρ/Unitless	0.039	–	0.040368(94)	0.037	0.03753(10)
β/°	35.090	–	33.657(62)	39.550	37.08(10)
V_3 [d]/cm^{-1}	532.407	593.5(89)	572.59(14)	464.367	508.05(22)
I_α [e]/uÅ^2	3.17	3.038(56)	3.2177(53)	3.16	3.1379(86)
ΔE_{E-A} [e]/MHz	–	–	52.251(94)	–	107.09(19)
$\angle(i,a)$ [e]/°	58.692	57.68(61)	57.463(61)	62.455	60.462(93)
$\angle(i,b)$ [e]/°	31.308	–	32.537(61)	27.545	29.538(93)
$\angle(i,c)$ [e]/°	90.00	–	[90.00] [f]	90.00	[90.00] [f]
J_{min}/J_{max}	–	2/38	2/53	–	24/53
K_a^{min}/K_a^{max}	–	0/11	0/36	–	0/25
${}^AN/{}^EN$ [g]	–	50/50	468/531	–	206/213
σ_{fit} [h]/MHz	–	–	0.036	–	0.043
σ_w [i]/Unitless	–	–	1.081	–	1.263

Notes. [a]Parameters estimated at the DFT/B3LYP/6-311++G(2d,3p) level of theory. [b]The numbers in parentheses are 1σ uncertainties in units of the last decimal digits. The ERHAM program (Groner 1997) was used for the analysis. [c]Fixed to the calculated value, which is usually a preferred constraint against the zero or poorly determined value (Urban & Sarka 1990). [d]Obtained from the XIAM (Hartwig & Dreizler 1996) analysis of solely non-overlapped rotational transitions. [e]Derived parameter. I_α is the moment of inertia of the methyl top, ΔE_{E-A} is the torsional energy difference, and $\angle(i,a/b/c)$ are the angles between the internal rotation axis i and the principal axes a, b, c. [f]Fixed value due to C_s symmetry. [g]Number of the *A*- and *E*-symmetry components in the fit. [h]Root mean square deviation of the fit. [i]Weighted deviation of the fit.

force field calculations were carried out using very tight convergence criteria and an ultra-fine integration grid and were all performed at the DFT/B3LYP/6-311++G(2d,3p) level of theory using the Gaussian16 program package (Frisch et al. 2016). Additionally, estimations of internal rotation barriers for both forms were calculated by varying the dihedral angle C–C–C–H by 2° while the rest of the coordinates were floated. A set of computed molecular parameters is given in Table 1.

4. Spectral analysis

4.1. *Z* isomer

Since the *Z* isomer ground state rotational spectrum has been studied by Groner et al. (1987), the initial assignments of the most intense low-K_a series were made based on the prediction with the constants from that study and aided by the Loomis-Wood-type plots obtained from the Assignment and Analysis of Broadband Spectra program package (Kisiel et al. 2005). In concordance with the magnitude of dipole moment components ($|\mu_a|$ = 1.806(6) D and $|\mu_b|$ = 0.759(21) D from Groner et al. 1987 and μ_c = 0.00 D from C_s symmetry), the spectrum is dominated by intense *a*-type *R*-branch transitions. A lower value of μ_b resulted in an overall poor signal-to-noise ratio of *b*-type transitions, and thus only a few weak ${}^bR$ and ${}^bQ$ transitions were identified and included in the dataset. Another characteristic feature of the spectrum is the *A*–*E* splitting of rotational transitions arising from the hindered internal rotation of the methyl group. However, due to the relatively high barrier to internal rotation (see Table 1), the *A*- and *E*-symmetry components of the $K_a < 6$ ${}^aR$-transition series were blended (see Fig. 3). The magnitude of the splittings gradually increased with increasing K_a and reached approximately 2.5 MHz. Frequent blends were also observed due to unresolved asymmetry splittings. The hyperfine structure of rotational transitions arising from the nuclear quadrupole coupling interactions of two ^{14}N

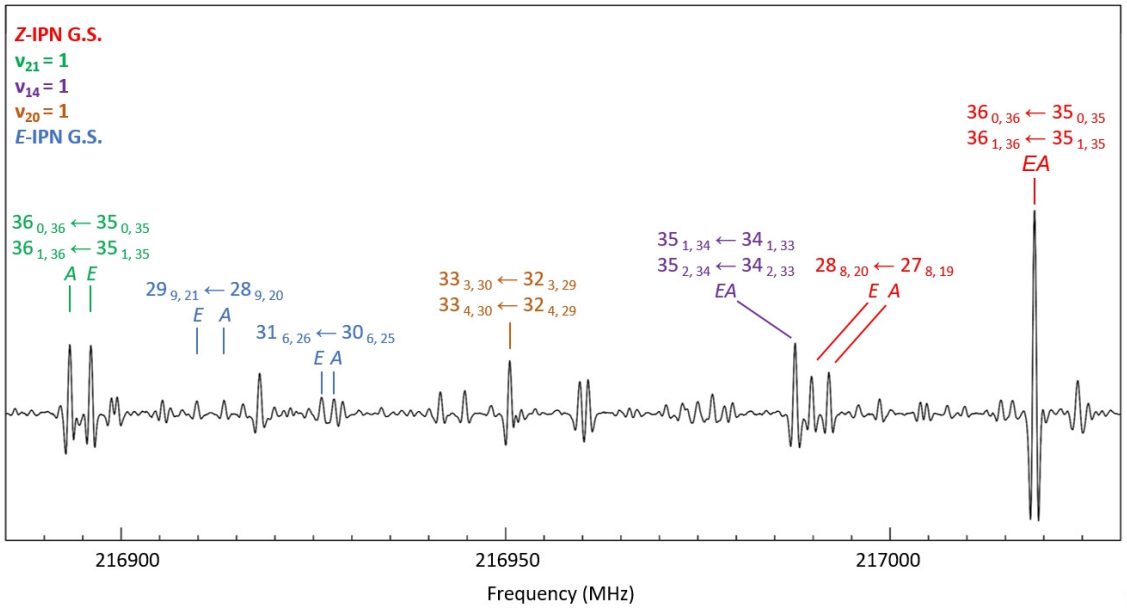


Fig. 3. Portion of the millimetre-wave spectrum displaying *a*-type rotational transitions of the *Z* isomer in the ground state and the three lowest-lying vibrationally excited states, and the *E* isomer in its ground state.

Table 2. Comparison of the changes in the rotational constants and inertial defects, $\Delta = I_c - I_b - I_a$, of *Z*-IPN in its ground and lowest-lying vibrationally excited states and *E*-IPN in the ground state derived from the calculated and experimentally determined rotational constants.

	Estimated					Experimental				
Parameters	*Z*-G.S.	$v_{21}=1$	$v_{14}=1$	$v_{20}=1$	*E*-G.S.	*Z*-G.S.	$v_{21}=1$	$v_{14}=1$	$v_{20}=1$	*E*-G.S.
$A_i - A_0$/MHz	0.0	–12.74	–0.18	25.09	–32.32	0.0	–11.64	–5.18	29.12	–30.22
$B_i - B_0$/MHz	0.0	–4.74	16.76	8.36	19.61	0.0	–5.25	17.49	8.80	21.09
$C_i - C_0$/MHz	0.0	–1.47	1.86	7.79	7.05	0.0	–1.62	2.19	8.13	8.04
Δ /uÅ^2	–2.89	–3.01	–2.51	–2.95	–2.89	–2.89	–3.01	–2.53	–2.94	–2.89

nuclei was unresolved in our spectra. However, for certain transitions these interactions manifested themselves in asymmetric line-shapes. These transitions were excluded from the fit.

To analyse the *A* and *E* components simultaneously, the ERHAM (Effective Rotational HAMiltonian) program (Groner 1997) with the *A*-reduced Hamiltonian in I^r representation (Watson 1977) was employed. The self-written MATLAB (MATrix LABoratory) program (MATLAB 2020) was used to convert the conventional labels *J*, K_a, and K_c to the labels used in ERHAM, *J* and *N* ($N = K_a - K_c + J + 1$), and also to calculate coefficients of the linear combinations of blended transitions required in ERHAM input files. Approximately 900 newly measured transitions up to $J = 53$ and $K_a = 36$ were combined with the microwave data from Groner et al. (1987) and fitted to the rotational and centrifugal distortion constants and the internal rotation parameters from Table 1. The sextic centrifugal distortion constants Φ_K and ϕ_J were not determined with satisfactory uncertainties and were thus fixed at their predicted values. Finally, an additional fit was performed using the XIAM program (Hartwig & Dreizler 1996) to obtain information about the barrier height. Since this program does not allow for a proper weighing of blended transitions, only the resolved *A*- and *E*-symmetry components were taken into consideration in this case. The analysis provided the barrier height shown in Table 1. The complete set of molecular parameters obtained from XIAM is given in Table A.1.

Further analysis of the spectrum revealed several satellites around each ground state line that might be assigned to transitions in vibrationally excited states. Indeed, our quantum-chemical calculations predicted three low-frequency vibrational modes, ν_{21}, ν_{14}, and ν_{20}, which are associated with the methyl torsion and the C–C≡N in-plane and out-of-plane bending motions, respectively. Their first excitations are predicted at 154.5, 190.2, and 271.8 cm^{-1} above the ground state, respectively (see Table A.2), and might be thus sufficiently populated at the room temperature of the experiment. Calculated vibration–rotation changes in rotational constants relative to the ground state are presented in Table 2 and were used to guide the assignments of the rotational transitions in these excited vibrational states.

Intense *A*–*E* doublets were observed for $v_{21} = 1$ (Fig. 3). As expected, the separation between *A* and *E* components was larger than for the corresponding transitions in the ground state and increased rapidly with K_a up to tens of megahertz. On the other hand, the rotational transitions in $v_{14} = 1$ revealed *A*–*E* splittings similar in magnitude to those in the ground state. Departures of many rotational transitions from their predicted frequencies were observed in both states in the highest frequency region of our spectrum even though it was clear from the Loomis-Wood-type plots that the assignments were correct. Such frequency shifts might imply resonance interactions of these vibrational states as they are close in energy. Since the perturbation analysis

Table 3. Spectroscopic parameters for the three lowest-lying vibrationally excited states of the Z isomer of IPN (A reduction, I^r representation).

Parameters	$v_{21} = 1$ [a]	$v_{14} = 1$ [a]	$v_{20} = 1$ [b]
A/MHz	9800.5361(90) [c]	9807.001(10)	9841.302(80)
B/MHz	4162.9793(16)	4185.7215(11)	4177.026(16)
C/MHz	2973.55144(47)	2977.36235(61)	2983.30376(39)
Δ_J/kHz	0.77110(69)	0.80414(47)	0.7726(79)
Δ_{JK}/kHz	15.3572(52)	15.2967(74)	15.91(14)
Δ_K/kHz	–6.205(69)	–5.270(84)	[–4.952] [e]
δ_J/kHz	0.25778(36)	0.27245(24)	0.2545(40)
δ_K/kHz	8.6859(70)	9.9309(70)	9.399(22)
Φ_J/mHz	[0.526] [d]	[0.526] [d]	[0.356] [e]
Φ_{JK}/Hz	0.1149(39)	0.1748(43)	[0.131] [e]
Φ_{KJ}/Hz	–0.2739(77)	–0.383(13)	[–0.278] [e]
Φ_K/Hz	[0.191] [e]	[0.191] [e]	[0.191] [e]
ϕ_J/mHz	[0.180] [e]	[0.180] [e]	[0.180] [e]
ϕ_{JK}/Hz	0.0716(22)	0.0728(24)	[0.067] [e]
ϕ_K/Hz	[0.361] [d]	[0.361] [d]	[0.296] [e]
ϵ_{10}/MHz	721.26(15)	–18.97(18)	–
ϵ_{20}/MHz	0.699(51)	–0.619(63)	–
$[(B-C)/4]_{10}$/kHz	–5.99(25)	–	–
$[(B+C)/2]_{10}$/kHz	–6.36(55)	–	–
$[\Delta_{JK}]_{10}$/Hz	8.83(68)	–	–
$[\delta_K]_{10}$/Hz	38.9(10)	–	–
ρ/Unitless	0.040309(22)	0.03304(31)	–
β/°	33.058(24)	45.80(26)	–
I_α [f]/uÅ^2	3.1876(28)	3.096(21)	–
ΔE_{E-A} [f]/MHz	–2165.89(48)	58.80(43)	–
$\angle(i,a)$ [f]/°	56.870(24)	67.46(19)	–
$\angle(i,b)$ [f]/°	33.130(24)	22.54(19)	–
$\angle(i,c)$ [f]/°	[90.00] [g]	[90.00] [g]	
J_{min}/J_{max}	23/53	23/53	24/53
K_a^{min}/K_a^{max}	0/21	0/18	0/7
${}^AN/{}^EN$ [h]	235/222	165/150	121 [i]
σ_{fit} [j]/MHz	0.043	0.035	0.041
σ_w [k]/Unitless	1.105	0.961	0.815

Notes. [a]The ERHAM program (Groner 1997) was used for the analysis. [b]The SPFIT/SPCAT program package (Pickett 1991) was used for the analysis. [c]The numbers in parentheses are 1σ uncertainties in units of the last decimal digits. [d]Fixed to the experimentally determined value of the ground state. [e]Fixed to the predicted value of the ground state, which is usually a preferred constraint against the zero or poorly determined value (Urban & Sarka 1990). [f]Derived parameter. I_α is the moment of inertia of the methyl top, ΔE_{E-A} is the torsional energy difference, and $\angle(i,a/b/c)$ are the angles between the internal rotation axis i and the principal axes a, b, c. [g]Fixed value due to C_s symmetry. [h]Number of the A- and E-symmetry components in the fit. [i]Number of rotational transitions with unresolved A-E splitting. [j]Root mean square deviation of the fit. [k]Weighted deviation of the fit.

is beyond the scope of the present investigations, only the less perturbed transitions were considered in the fitting procedure. They include series up to $K_a = 6$ and $K_a = 4$ for $v_{21} = 1$ and $v_{14} = 1$, respectively. Nevertheless, transitions up to $K_a = 21$ and $K_a = 18$, respectively, could be analysed well at lower frequencies. The analysis of the measured transitions was performed using the ERHAM program, and the obtained spectroscopic parameters are given in Table 3.

For the last excited vibrational state, $v_{20} = 1$, only the rotational transitions with unresolved A–E splittings were assigned and fitted up to $K_a = 7$ due to the rapidly diminishing intensities when A- and E-symmetry components are completely resolved. For this reason, the observed transitions were treated using the purely rotational Hamiltonian employing the SPFIT program package (Pickett 1991). The obtained spectroscopic constants are listed in Table 3. A list of measured transitions for the Z isomer is provided in Table A.3.

Table 4. Values of rotational partition functions for the ground state of Z-IPN and E-IPN.

T (K)	Z isomer	E isomer
300.000	636647	635117
225.000	413469	412479
150.000	224957	224422
75.000	79509	79320
37.500	28119	28052
18.750	9952	9928
9.375	3527	3518

4.2. E isomer

After the assignment of the rotational lines corresponding to Z-IPN, the search for the E isomer transitions was performed. This less stable isomer is predicted at 494.5 cm^{-1} above the Z isomer, and its expected Boltzmann population at 298.15 K is approximately 8.4%. Nevertheless, based on the rather large dipole moment components ($|\mu_a| = 4.27$ D, $|\mu_b| = 2.13$ D, and $|\mu_c| = 0.00$ D from DFT calculations) and the predicted barrier height ($V_3 = 464.4$ cm^{-1}), low-K_a series of a-type R-branch transitions with unresolved A–E splittings were anticipated to appear in the spectrum with intensities similar to those from $v_{20} = 1$. These transitions were found close to those corresponding to the excited state $v_{20} = 1$ and were gradually assigned and fitted up to $J = 53$ and $K_a = 25$. Unfortunately, no b-type transitions were observed for the E isomer because of their insufficient intensities. As in the case of the Z isomer ground state, the ERHAM program was used to determine the spectroscopic constants from Table 1 and the XIAM code was employed to evaluate the threefold barrier $V_3 = 508.05(22)$ cm^{-1}. The remaining parameters from the latter analysis can be found in Table A.1, and the measured transitions are listed in Table A.4.

4.3. Rotational partition functions

Rotational partition functions for both isomers in the ground vibrational state were calculated at seven temperatures using ERHAM. The rotational states up to $J = 120$ were included, and the resulting Q_{rot} values are listed in Table 4. These numerical values agree well with a rigid asymmetric rotor approximation given by Eq. (3.69) in Gordy & Cook (1984) multiplied by the total spin weight $(2I+1)^3 = 8$ ($I = 1/2$) and divided by the symmetry number, which for the C_s point group equals 1.

5. Discussion

The present work provides a significant improvement over the previous microwave study (Groner et al. 1987) as it greatly extends the covered ranges of frequencies and quantum numbers. The rotational and quartic centrifugal distortion constants obtained for the Z isomer in its ground vibrational state agree with those reported by Groner et al. (1987), and moreover, most

of them are more precise, by up to two orders in magnitude (see Table 1). The newly determined sextic centrifugal distortion constants are in good agreement with the corresponding calculated values. As for the internal rotation parameters, a slight decrease in the barrier height is perceptible in comparison with Groner et al. (1987) and is very likely caused by a strong correlation between V_3 and I_α. We note that when the data from Groner et al. (1987) are re-fitted keeping the I_α fixed at the theoretical value of 3.17 uÅ^2, which falls into the range typically found in molecules exhibiting methyl top internal rotation (Demaison et al. 1987), the barrier height changes to 571.2(18) cm^{-1}, which is very close to the value determined from the present analysis (see Table A.5). Also, the ϵ_{10} value obtained from the ERHAM analysis is reasonably close to the values found for other molecules with sufficiently high barriers (Lengsfeld et al. 2021).

Additionally, this work provides the first experimental evidence of the less stable E isomer. Figure 1 illustrates that both forms differ from each other, mainly in the position of the imino hydrogen, which results in very similar molecular constants for both species. Consequently, the E isomer ground state could be easily mistaken for one of the vibrationally excited states of the Z form. To avoid such a misinterpretation, we carefully considered three different criteria. First, experimental differences between the rotational constants for the E and Z isomer were compared with those for the excited vibrational states of the Z isomer and their quantum-chemical counterparts. Table 2 shows that these experimental differences are only consistent with those predicted for the E isomer and provide solid proof for its correct identification. The inertial defect values were taken as the second criterion. As expected, the inertial defects for the Z and E isomer ground states are identical, whereas more negative values with respect to the Z isomer ground state are observed for the $v_{21} = 1$ and $v_{20} = 1$ excited vibrational states. These findings further confirm that these states originate from out-of-plane vibrational motions. Finally, the differences between the predicted and experimentally determined barrier heights of -40.5 cm^{-1} and -43.7 cm^{-1} for the Z and E isomer, respectively, are mutually consistent and further support the present assignment of the E-IPN ground state.

6. Conclusions

The new millimetre-wave study of IPN was performed up to 329 GHz and substantially extends the current knowledge of the rotational spectrum over the previous microwave study. More than 1700 A and E state transitions of the Z isomer in the ground vibrational state and in the three lowest-lying vibrationally excited states, $\nu_{21} = 1$, $\nu_{14} = 1$, and $\nu_{20} = 1$, were measured and assigned. Additionally, this work reports the first assignment of rotational transitions of the less stable E isomer in the ground vibrational state. The joint analysis of the internal motion with the ERHAM and XIAM programs yielded accurate spectroscopic parameters, including the threefold barrier heights for both isomers, which reproduce the dense rotational spectrum well. The most intense rotational transitions observed at the room-temperature laboratory measurements were included in the fit, ensuring reliable support for future astronomical searches at the lower temperatures typical of interstellar environments.

Acknowledgements. Financial support was acquired from the Czech Science Foundation (GACR, grant No. 19-25116Y). L.K., K.L., J.K., and K.V. gratefully acknowledge this financial support. L.K., J.K., K.L., and P.K. thank the financial support from the Ministry of Education, Youth and Sports of the Czech Republic (MSMT) within the Mobility grant No. 8J21FR006. K.L. appreciates the financial support from the Specific university research – grant A2_FCHI_2021_023. Computational resources were supplied by the project e-Infrastruktura CZ (e-INFRA CZ ID:90140) supported by the Ministry of Education, Youth and Sports of the Czech Republic. Access to CESNET storage facilities provided by the project e-INFRA CZ under the programme Projects of Large Research, Development, and Innovations Infrastructures LM2018140), is also appreciated. J.-C.G. and L.K. acknowledge support by the Barrande project No. 46662VH. J.-C.G. thanks the financial support from the Centre National d'Etudes Spatiales (CNES, France; grant number 4500065585) and the Programme National Physique et Chimie du Milieu Interstellaire (PCMI) of CNRS/INSU with INC/INP, France co-funded by CEA, France and CNES.

References

Balucani, N. 2009, IJMS, 10, 2304
Belloche, A., Menten, K. M., Comito, C., et al. 2008, A&A, 482, 179
Belloche, A., Garrod, R. T., Müller, H. S. P., & Menten, K. M. 2014, Science, 345, 1584
Bernstein, M. P., Dworkin, J. P., Sandford, S. A., Cooper, G. W., & Allamandola, L. J. 2002, Nature, 416, 401
Buchanan, Z., Lee, K. L. K., Chitarra, O., et al. 2021, J. Mol. Spectr., 377, 111425
Cabezas, C., Bermúdez, C., Endo, Y., Tercero, B., & Cernicharo, J. 2020, A&A, 636, A33
Demaison, J., Maes, H., Van Eijck, B. P., Wlodarczak, G., & Lasne, M. C. 1987, J. Mol. Spectr., 125, 214
Durig, J. R., Zhou, S. X., Zhou, C. X., & Durig, N. E. 2010, J. Mol. Struct., 967, 1
Frisch, M. J., Trucks, G. W., Schlegel, H. B., et al. 2016, Gaussian 16 Revision C.01 (USA: Auburn University)
Garrod, R. T., Weaver, S. L. W., & Herbst, E. 2008, ApJ, 682, 283
Garrod, R. T., Müller, H. S. P., Menten, K. M., Comito, C., & Schilke, P. 2009, A&A, 499, 215
Gordy, W., & Cook, R. L. 1984, Microwave Molecular Spectra (New York: Wiley Interscience)
Groner, P. 1997, J. Chem. Phys., 107, 4483
Groner, P., Gunde, R., Ha, T.-K., & Bauder, A. 1987, Chem. Phys. Lett., 139, 479
Hartwig, H., & Dreizler, H. 1996, Zeitschrift für Naturforschung A, 51, 923
Herbst, E., & van Dishoeck, E. F. 2009, ARA&A, 47, 427
Kania, P., Stříteská, L., Šimečková, M., & Š. Urban. 2006, J. Mol. Struct., 795, 209
Kisiel, Z., Pszczółkowski, L., Medvedev, I. R., et al. 2005, J. Mol. Spectr., 233, 231
Kolesniková, L., León, I., et al. 2021, Angew. Chem. Int. Ed., 60, 24461
Lee, K. L. K., Changala, P. B., Loomis, R. A., et al. 2021a, ApJ, 910, L2
Lee, K. L. K., Loomis, A. R., Burkhardt, A. M., et al. 2021b, ApJ, 908, L11
Lengsfeld, K. G., Buschmann, P., Dohrmann, F., & Grabow, J.-U. 2021, J. Mol. Spectr., 377, 111441
Loomis, R. A., Burkhardt, A. M., Shingledecker, C. N., et al. 2021, Nat. Astron., 5, 188
MATLAB. 2020, version 9.8.0.1451342 (R2020a) (Natick, Massachusetts: The MathWorks Inc.)
McCarthy, M. C., Lee, K. L. K., Loomis, R. A., et al. 2021, Nat. Astron., 5, 176
McGuire, B. A. 2022, ApJS, 259, 30
McGuire, B. A., Burkhardt, A. M., Kalenskii, S., et al. 2018, Science, 359, 202
McGuire, B. A., Burkhardt, A. M., Loomis, R. A., et al. 2020, ApJ, 900, L10
McGuire, B. A., Loomis, R. A., Burkhardt, A. M., et al. 2021, Science, 371, 1265
McNaughton, D., Jahn, M. K., Travers, M. J., et al. 2018, MNRAS, 476, 5268
Melosso, M., Melli, A., Puzzarini, C., et al. 2018, A&A, 609, A121
Motiyenko, R. A., Armieieva, I. A., Margulès, L., Alekseev, E. A., & Guillemin, J.-C. 2019, A&A, 623, A162
Pickett, H. M. 1991, J. Mol. Spectr., 148, 371
Powner, M. W., Sutherland, J. D., & Szostak, J. W. 2010, JACS, 132, 16677
Rivilla, V. M., Martín-Pintado, J., Jiménez-Serra, I., et al. 2019, MNRAS, 483, L114
Sanz-Novo, M., León, I., Alonso, J. L., Largo, A., & Barrientos, C. 2020, A&A, 644, A3
Sanz-Novo, M., León, I., Alonso, E. R., Kolesniková, L., & Alonso, J. L. 2021, ApJ, 915, 76
Takano, S., Sugie, M., Sugawara, K., et al. 1990, J. Mol. Spectr., 141, 13
Urban, Š., & Sarka, K. 1990, J. Mol. Spectr., 144, 446
Watson, J. K. G. 1977, in Vibrational Spectra and Structure, ed. J. R. Durig (Amsterdam: Elsevier), 6, 1
Zaleski, D. P., Seifert, N. A., Steber, A. L., et al. 2013, ApJ, 765, L10
Zdanovskaia, M. A., Dorman, P. M., Orr, V. L., et al. 2021, JACS, 143, 9551
Zeng, S., Quénard, D., Jiménez-Serra, I., et al. 2019, MNRAS, 484, L43

Appendix A: Complementary tables

Table A.1 presents the molecular parameters for the *Z* and *E* isomers obtained from the XIAM analysis performed on the isolated non-overlapped rotational transitions. Table A.2 presents the anharmonic frequencies of normal vibrational modes of *Z*-IPN and *E*-IPN calculated at the DFT/B3LYP/6-311++G(2d,3p) level of theory. Table A.3 presents a list of measured transitions of *Z*-IPN in its ground vibrational state and three lowest-lying vibrationally excited states. Table A.4 presents a list of measured transitions of *E*-IPN. Table A.5 presents data from Groner et al. (1987) re-fitted in XIAM with I_α kept fixed at the theoretical value.

Table A.1. Molecular parameters for the *Z* and *E* isomer obtained from the XIAM analysis performed on the isolated non-overlapped rotational transitions.

Parameters	*Z* isomer	*E* isomer
A / MHz	9812.1817(25)[a]	9781.901(11)
B / MHz	4168.29145(24)	4189.37174(75)
C / MHz	2975.10391(31)	2983.1566(15)
Δ_J / kHz	0.77314(29)	0.76878(52)
Δ_{JK} / kHz	15.6681(15)	15.0022(37)
Δ_K / kHz	–5.873(28)	–5.920(56)
δ_J / kHz	0.25747(13)	0.25119(22)
δ_K / kHz	9.4476(51)	8.979(11)
Φ_J / mHz	[0.356][b]	[0.324]
Φ_{JK} / Hz	0.1507(47)	0.17281(90)
Φ_{KJ} / Hz	–0.333(16)	–0.4010(39)
Φ_K / Hz	[0.191][b]	[0.132][b]
ϕ_J / mHz	[0.180][b]	[0.158][b]
ϕ_{JK} / Hz	0.0694(13)	0.0566(22)
ϕ_K / Hz	0.364(33)	[0.269][b]
Dpi_{2-} / MHz	0.203(21)	0.465(34)
V_3 / cm^{-1}	572.59(14)	508.05(22)
F_0 / MHz	[159.430][b]	[159.930][b]
$I_\alpha{}^c$ / uÅ^2	[3.17][b]	[3.16][b]
$\angle(i,a)^c$ / °	57.818(50)	61.682(97)
$\angle(i,b)^c$ / °	32.182(50)	28.318(97)
$\angle(i,c)^c$ / °	[90.00][d]	[90.00][d]
$J_{\min}/J_{\max}$	2 / 46	24 / 46
$K_a^{\min}/K_a^{\max}$	1 / 16	0 / 25
${}^A N/{}^E N^e$	192 / 303	110 / 149
$\sigma_{\text{fit}}{}^f$ / MHz	0.036	0.052
$\sigma_{\text{w}}{}^g$ / Unitless	1.054	1.594

Notes. [(a)]The numbers in parentheses are 1σ uncertainties in units of the last decimal digits. [(b)]Fixed to the calculated value, which is usually a preferred constraint against the zero or poorly determined value (Urban & Sarka 1990). [(c)]Derived parameter. [(d)]Fixed value due to C_s symmetry. [(e)]Number of *A*- and *E*-symmetry components in the fit. [(f)]Root mean square deviation of the fit. [(g)]Weighted deviation of the fit.

Table A.2. Anharmonic frequencies of normal vibrational modes of *Z*-IPN and *E*-IPN calculated at the DFT/B3LYP/6-311++G(2d,3p) level of theory.

	Z isomer		*E* isomer	
Mode	Frequency (cm^{-1})	Symmetry	Frequency (cm^{-1})	Symmetry
1	3299.6	A'	3278.4	A'
2	3004.8	A'	2990.9	A'
3	2936.6	A'	2932.9	A'
4	2283.5	A'	2296.9	A'
5	1644.3	A'	1650.0	A'
6	1433.9	A'	1440.2	A'
7	1382.6	A'	1377.0	A'
8	1305.7	A'	1313.8	A'
9	1090.9	A'	1074.4	A'
10	981.7	A'	969.4	A'
11	730.3	A'	734.7	A'
12	603.0	A'	603.4	A'
13	426.3	A'	435.0	A'
14	190.2	A'	195.1	A'
15	2952.4	A''	2956.5	A''
16	1431.2	A''	1425.5	A''
17	1058.0	A''	1057.0	A''
18	916.6	A''	893.0	A''
19	569.1	A''	581.1	A''
20	271.8	A''	275.9	A''
21	154.5	A''	139.5	A''

Table A.3. List of measured transitions of *Z*-IPN in its ground vibrational state and the three lowest-lying vibrationally excited states.

State	Symmetry	J'	K_a'	K_c'	J''	K_a''	K_c''	ν_{obs}[(a)] (MHz)	$\nu_{obs} - \nu_{calc}$[(b)] (MHz)	u_{obs}[(c)] (MHz)	$(\nu_{obs} - \nu_{calc})_{blends}$[(d)] (MHz)	Weight[(e)]	Note[(f)]
Ground state	E	27	8	19	27	8	20	22716.2780	0.0180	0.030	-	-	(1)
	A	27	8	19	27	8	20	22719.6380	–0.0140	0.030	-	-	(1)
	A	36	0	36	35	0	35	217018.7916	0.0331	0.050	–0.0118	0.25	(2)
	A	36	1	36	35	1	35	217018.7916	0.0331	0.050	–0.0118	0.25	(2)
	E	36	0	36	35	0	35	217018.7916	0.0331	0.050	0.0780	0.25	(2)
	E	36	1	36	35	1	35	217018.7916	0.0331	0.050	0.0780	0.25	(2)
$v_{21} = 1$	A	36	0	36	35	0	35	216893.3205	0.0369	0.050	0.0369	0.50	(2)
	A	36	1	36	35	1	35	216893.3205	0.0369	0.050	0.0369	0.50	(2)
	E	36	0	36	35	0	35	216896.0573	0.0356	0.050	0.0356	0.50	(2)
	E	36	1	36	35	1	35	216896.0573	0.0356	0.050	0.0356	0.50	(2)
$v_{14} = 1$	A	35	1	34	34	1	33	216987.6513	0.0118	0.050	–0.1333	0.25	(2)
	A	35	2	34	34	2	33	216987.6513	0.0118	0.050	–0.1333	0.25	(2)
	E	35	1	34	34	1	33	216987.6513	0.0118	0.050	0.1570	0.25	(2)
	E	35	2	34	34	2	33	216987.6513	0.0118	0.050	0.1570	0.25	(2)
$v_{20} = 1$	-	33	3	30	32	3	29	216950.5403	0.0828	0.050	0.0334	0.50	(2)
	-	33	4	30	32	4	29	216950.5403	–0.0160	0.050	0.0334	0.50	(2)

Notes. [(a)]Observed frequency. [(b)]Observed minus calculated frequency. [(c)]Uncertainty of the observed frequency. [(d)]Observed minus calculated frequency for blends. [(e)]Intensity weighting factor for blended transitions. [(f)]Source of data: (1) Groner et al. (1987), (2) This work. This table is available in its entirety in electronic form at the CDS. A portion is shown here for guidance regarding its form and content.

Table A.4. List of measured transitions of *E*-IPN.

State	Symmetry	J'	K_a'	K_c'	J''	K_a''	K_c''	ν_{obs}[(a)] (MHz)	$\nu_{obs} - \nu_{calc}$[(b)] (MHz)	u_{obs}[(c)] (MHz)	$(\nu_{obs} - \nu_{calc})_{blends}$[(d)] (MHz)	Weight[(e)]	Note[(f)]
Ground state	E	29	9	21	28	9	20	216909.8430	0.0085	0.030	-	-	(2)
	A	29	9	21	28	9	20	216913.3793	0.0250	0.030	-	-	(2)
	E	31	6	26	30	6	25	216926.0656	–0.0300	0.030	-	-	(2)
	A	31	6	26	30	6	25	216927.6773	–0.0145	0.030	-	-	(2)

Notes. [(a)]Observed frequency. [(b)]Observed minus calculated frequency. [(c)]Uncertainty of the observed frequency. [(d)]Observed minus calculated frequency for blends. [(e)]Intensity weighting factor for blended transitions. [(f)]Source of data: (1) Groner et al. (1987), (2) This work. This table is available in its entirety in electronic form. A portion is shown here for guidance regarding its form and content.

Table A.5. Data for the *Z* isomer taken from Groner et al. (1987) and re-fitted in XIAM with I_α fixed at the theoretical value of 3.17 uÅ^2 to eliminate the strong correlation between V_3 and I_α.

Parameters	This work
A / MHz	9812.1276(57) [a]
B / MHz	4168.2903(11)
C / MHz	2975.1062(11)
Δ_J / kHz	[0.859] [b]
Δ_{JK} / kHz	15.27(16)
Δ_K / kHz	–4.77(76)
δ_J / kHz	0.2527(53)
δ_K / kHz	9.313(93)
V_3 / cm^{-1}	571.2(18)
F_0 / MHz	[159.430][c]
I_α [d] / uÅ^2	[3.17][c]
$\angle(i,a)^d$ / °	32.69(44)
$\angle(i,b)^d$ / °	57.31(44)
$\angle(i,c)^d$ / °	90.00[e]
$J_{\min}/J_{\max}$	8 / 38
$K_a^{\min}/K_a^{\max}$	1 / 11
${}^AN/{}^EN^f$	26 / 26
$\sigma_{\text{fit}}{}^g$ / MHz	0.031
$\sigma_{\text{w}}{}^h$ / Unitless	1.048

Notes. [a]The numbers in parentheses are 1σ uncertainties in units of the last decimal digits. [b]Fixed to the value reported in Groner et al. (1987). [c]Fixed to the value calculated in this paper at the DFT/B3LYP/6-311++G(2d,3p) level of theory. [d]Derived parameter. [e]Fixed value due to C_s symmetry. [f]Number of *A*- and *E*-symmetry components in the fit. [g]Root mean square deviation of the fit. [h]Weighted deviation of the fit.